Available online at www.sciencedirect.com
ScienceDirect
Trans. Nonferrous Met. Soc. China 29(2019) 1138−1151
Transactions of Nonferrous Metals Society of China
www.tnmsc.cn

Modeling of dynamic recrystallization volume fraction evolution for AlCu4SiMg alloy and its application in FEM

Guo-zheng QUAN[1], Rui-ju SHI[1], Jiang ZHAO[1], Qiao LIU[1], Wei XIONG[2], Hui-min QIU[1]

1. State Key Laboratory of Mechanical Transmission,
School of Material Science and Engineering, Chongqing University, Chongqing 400044, China;
2. Institute of Nuclear and New Energy Technology,
Collaborative Innovation Center of Advanced Nuclear Energy Technology,
Key Laboratory of Advanced Reactor Engineering and Safety of Ministry of Education,
Tsinghua University, Beijing 100084, China

Received 4 April 2018; accepted 16 November 2018

Abstract: To improve the understanding of coupling effect between dynamic recrystallization (DRX) behaviors and flow behaviors of as-cast AlCu4SiMg, a finite element (FE) simulation equipped with the models of DRX evolution was implemented. A series of isothermal compression tests were performed primarily on a Gleeble−3500 thermo-mechanical simulator in a temperature range of 648−748 K and a strain rate range of 0.01−10 s^{-1}. According to the measured true stress−strain data, the strain hardening rate curves ($d\sigma/d\varepsilon$ versus σ) were plotted to identify the critical strains for DRX initiation (ε_c). By further derivation of the related material constants, the DRX volume fraction equation and the strain for 50% DRX ($\varepsilon_{0.5}$) equation were solved. Accordingly, the aforementioned DRX equations were implanted into the FE model to conduct a series of simulations for the isothermal compression tests. The results show that during the evolution of DRX volume fraction at a fixed strain rate, the strain required for the same amount of DRX volume fraction increases with decreasing temperature. In contrast, at a fixed temperature, it increases with increasing strain rate. Ultimately, the DRX kinetics model of AlCu4SiMg alloy and the consequence of the FE analysis were validated by microstructure observations.

Key words: AlCu4SiMg alloy; DRX kinetics model; DRX volume fraction; flow behavior

1 Introduction

AlCu4SiMg, one of the most popular alloy of 2000-series aluminum alloys, has been widely used in aerospace industry in view of its high specific strength, superior high-temperature properties, resistance to fatigue crack propagation, and fracture toughness [1,2]. Generally, the products of AlCu4SiMg were manufactured by the hot forming process such as extrusion and forging, during which three metallurgical phenomena including work hardening (WH), dynamic recovery (DRV) and DRX occurred [3,4].

The microstructures and corresponding mechanical properties of products, in a large extent, are determined by the interaction of three above-mentioned metallurgical phenomena [5,6]. It is commonly believed that the occurrence of DRX is conducive to the grain refinement and homogenization, hence, the mechanical properties were improved correspondingly [4,7].

So, it is a significant issue to investigate how to take advantage of DRX for achieving the adjustment of microstructures. Moreover, during hot plastic deformation, the evolution of DRX is a continuous dynamic course related to the processing parameters such as temperature, strain rate and true strain. Nevertheless, it is extremely difficult to dynamically observe the DRX evolution process in a physical experiment, while the FE simulation equipped with the models of DRX evolution provides an efficient solution. In addition, the DRX kinetics model, the relationships between the DRX volume fraction and processing parameters, is the essential

Foundation item: Project (cstc2016jcyjA0335) supported by Chongqing Foundation and Frontier Research, China; Project (P2017-020) supported by Open Fund Project of State Key Laboratory of Materials Processing and Die & Mould Technology, China
Corresponding author: Guo-zheng QUAN; Tel: +86-15922900904; Fax: +86-23-65111493; E-mail: quangz3000@sina.com
DOI: 10.1016/S1003-6326(19)65022-3

portion of finite element model (FEM) for dynamically observing DRX evolution process of deformation materials. Hence, to improve the macro-mechanical properties of AlCu4SiMg products through adjusting the microstructures, a prepared DRX kinetics model with deformation conditions effect is indispensable.

QUAN et al [8,9] mentioned that the flow curves, a direct consequence of microstructural changes, directly reflected the hot working behaviors of alloys. According to the stress−strain data collected from a series of isothermal compressions, it is realizable to model the DRX kinetics. Over the last few decades, the researches about the modeling of DRX kinetics attracted vast investigators [10]. ZHOU et al [11] studied hot tensile deformation behaviors of Al−Zn−Mg−Cu alloy and developed the Arrhenius-type constitutive model to predict the peak stress under the tested deformation conditions. CAI et al [12] established DRX kinetic model of AZ41M magnesium alloy on the basis of Avrami equation to characterize the evolution of DRX volume fraction. WEN et al [13] proposed DRX kinetics models which quantitatively reveal the influences of initial δ phase upon the DRX behavior. CHEN et al [14] proposed a new method to establish DRX kinetics model, in which only the DRX volume fractions in the center part of deformed specimens need to be employed. Up till now, the FE simulation equipped with the DRX kinetics model has been widely used to guide the production of alloy parts. As for aluminum-based alloy, LI et al [15−17] investigated hot deformation behaviors, DHAL et al [18] and LI et al [19] focused on the influence factors on the grain growth mechanism of the recrystallized grains. KAIBYSHEV and MALOPHEYEV [7] reviewed the mechanisms of DRX operating at severe plastic deformation in a wide temperature range for aluminum alloys. TAJALLY and HUDA [20] analyzed the isothermal recrystallization kinetics for 7075 aluminum alloy within the framework of the Johnson−Mehl−Avrami−Kolmogorov equation. The researches for AlCu4SiMg focus on the hot deformation behaviors and the mechanisms of DRX, but few attentions have been paid to the modeling of DRX kinetics and its application in FEM. In this work, the main work is to investigate the hot deformation behaviors of AlCu4SiMg alloy based on experimental results from isothermal compression tests, and then the relevant DRX kinetics model including the temperature and strain rate effects was developed. Based on the finite element platform, the true stress−strain data and the developed DRX kinetics equation describing the microstructure evolutions were programed into finite element codes for establishing a simulation model, which is prepared for dynamically observing DRX evolution process of deformation materials. Ultimately, the DRX kinetics model of AlCu4SiMg alloy and the consequence of the FE analysis are validated by microstructure observations.

2 Experimental

The material selected in this work is AlCu4SiMg, whose detailed chemical compositions (wt.%) are as follows: 4.47 Cu, 0.63 Si, 0.58 Mg, 0.49 Mn, 0.23 Fe, 0.021 Zn, 0.021 V, 0.017 Ti, and balance Al. Twenty-one specimens with a diameter of 10 mm and a height of 12 mm were wire-electrode cut from the radial middle region of an as-cast cylindrical billet with a diameter of 360 mm and a height of 90 mm.

The compression experiment schedule considering strain rate and temperature effects was designed as follows: twenty specimens were compressed with a fixed height reduction of 60% resulting in a true strain of 0.916 under four strain rates of 0.01, 0.1, 1 and 10 s^{-1} at five temperatures of 648, 673, 698, 723 and 748 K. In this isothermal compression experiment, a Gleeble−3500 thermo-mechanical physical simulator was employed. It is a fully integrated digital closed loop control thermal and mechanical testing system. The direct resistance heating system in it with a thermo-coupled-feedback-controlled AC current provides rapid and precise temperature control.

Before the compression, two thermocouple wires were welded on the circumference of the specimen in the mid-height. Then the specimen was placed between two anvils, meanwhile two graphite foils with a diameter of 20 mm serving as a lubricant were placed between specimens and anvils. The hot compression test scheme is shown in Fig. 1. Each specimen was resistance heated to the proposed temperature at a heating rate of 10 K/s, and was held at a certain temperature for 180 s to decrease the material anisotropy. The temperature signals of this specimen were collected and transmitted to a computer for accurate monitoring and adjusting by the thermocouple wires. Subsequently, the specimen was compressed according to the pre-designed schedule. After the compression, the specimen was quenched by water as soon as possible to retain the high temperature

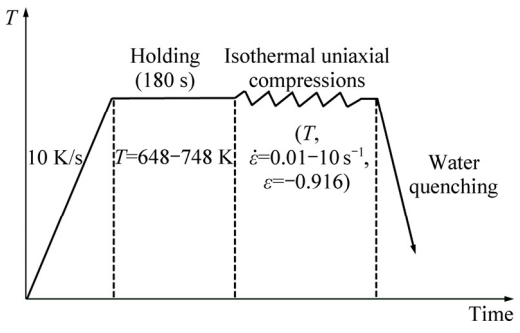

Fig. 1 Hot compression test scheme of AlCu4SiMg

microstructures. Besides the deformed specimens, one specimen without isothermal compression was remained for original grain morphology observation.

During the compression process, the nominal stress–strain data were monitored continuously by a computer equipped with an automatic data acquisition system. The true stress and true strain were derived from nominal stress−strain data according to the following formulas: $\sigma_T=\sigma_N(1-\varepsilon_N)$, $\varepsilon_T=\ln(1-\varepsilon_N)$, where σ_T is the true stress, ε_T is the true strain, σ_N is the nominal stress, and ε_N is the nominal strain [21,22].

After the compression experiment, all the twenty-one specimens were sectioned into two halves with their cylinder axes parallel to the compression axis direction by wire cutting. The sections were ground by abrasive papers of SiC, and were electro-polished at 25 V for 20 s in an electrolyte consisting of 30 mL C_2H_6O and 10 mL $HClO_4$. Then, the sections of all specimens were coated with anodic film in a solution consisting of 95 mL H_2O and 5 mL HBF_4. Finally, the microstructures of the prepared sections were observed by the metallographic microscope.

3 Flow behaviors and deformation mechanisms

3.1 Flow behavior

The true compressive stress−strain curves of as-cast AlCu4SiMg obtained at different deform conditions are presented in Fig. 2. The flow stress evolution along with strain exhibits three distinct stages [23]. At the first (WH) stage, the flow stress increases rapidly with the increase of strain. During the stage, the dominating metallurgical phenomenon is WH, which is caused by the generation and multiplication of dislocation. Meanwhile, the accompanying DRV caused by the annihilation of dislocations due to ease of cross slip, climb, and dislocation unpinning is too weak to exceed WH.

In the second (softening) stage, with the increase of strain, the gradually-accumulated energy at the grain boundaries augments rapidly to DRX activation energy, which facilitates the generation of equiaxed DRX grains. Subsequently, the DRX occupies a major role in softening mechanism, which leads to a slowdown in the upward trend of flow stress. When dynamic softening rate is equal to WH rate, flow stress reaches a peak value, and then exhibits a smaller and smaller decrease till a steady stage. In the third (extensive steady) stage, the flow stress maintains at a fairly constant level regardless the increase of strain.

From Fig. 2, it can be obviously found that the flow stress increases monotonically with increasing strain rate or decreasing deformation temperature, accordingly, lower levels of flow stress usually appear at higher temperatures and lower strain rates. This is mainly due to the fact that higher strain rate not only induces more tangled dislocation structures as barriers to dislocation movement but also decreases the growth and coalescence

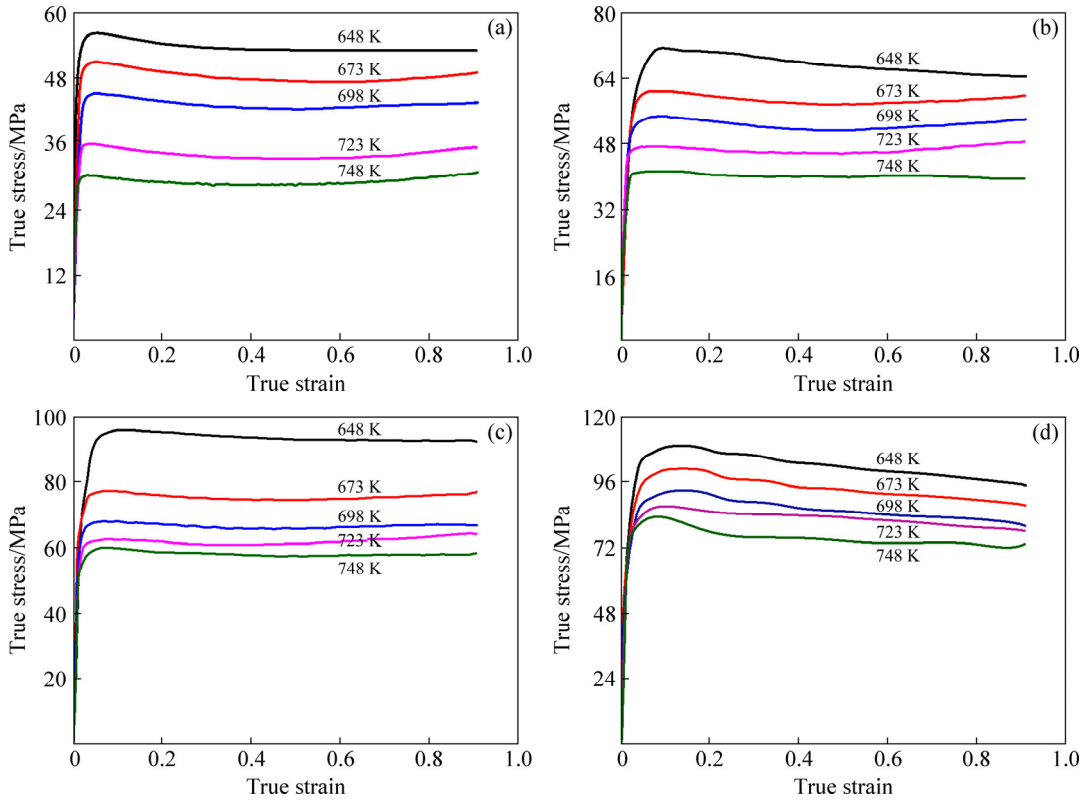

Fig. 2 True compressive stress−strain curves of as-cast AlCu4SiMg obtained at different deform temperatures with strain rates of 0.01 s^{-1} (a), 0.1 s^{-1} (b), 1 s^{-1} (c) and 10 s^{-1} (d)

time of microvoids or microcracks. Moreover, with the increase of the temperature, the grain boundary mobility for annihilating dislocations is promoted, meanwhile the dynamic softening is enhanced. When the strain rate rises to 10 s^{-1}, the flow stress curves at 648−698 K possess a wave phenomenon in time domain, which are identified as the Portevin-Le Chatelier (PLC) effect. The microcosmic mechanism accounting for PLC effect is dynamic strain aging caused by the dynamic comprehensive function of dislocations and solute atoms. A lot of investigators were attracted by the PLC effect, a multi-scale coupling issue, which involves macro-scopical deformation, micro-grain deformation and micro dislocation movement.

3.2 Deformation mechanism

AlCu4SiMg alloy is a typical FCC crystal, the basal slip systems of it are {110}, {112}, {123}, and all with the Burgers vector of <111>. During the hot deformation process, the dominant deformation mechanisms of AlCu4SiMg are solute drag creep and grain boundary sliding, which were examined and discussed as a function of temperature and strain [24]. In the first stage of deformation, the increasing dislocation density promotes the lattice strain increasing. As the degree of strain increases, the generation of the small-angle grain boundaries and medium-sized crystallites results in the decrease of dislocation density, as well as the decrease of lattice strain [25]. In addition, the dynamically precipitated dispersoids Al_3Zr and $Al_{20}Cu_2Mn_3$ pin dislocations resulting in the absence of dramatic softening behavior and the increase of deformation activation energy [26]. Meanwhile, continue dynamic recrystallization (CDRX) occurs at merged subgrain boundary because those particles pin grain boundary and retard boundary migration.

4 Constitutive modeling for DRX kinetics

4.1 Initiation of DRX

In order to characterize the evolution of DRX volume fraction, the Johnson–Mehl–Avrami–Kolmogorov (JMAK) type equation $X_{DRX}=1-\exp\left[-\beta_d\left(\frac{\varepsilon-\varepsilon_c}{\varepsilon_{0.5}}\right)^{k_d}\right]$ was adopted. It is associated with critical strain ε_c and the strain $\varepsilon_{0.5}$ corresponding to the recrystallization volume fraction of 50%, both of them are related to a number of parameters such as temperature, strain rate and grain size. The modeling of DRX kinetics based on the discrimination of critical conditions for the onset of DRX, which can be identified from $d\sigma/d\varepsilon$ versus σ curve, in which an inflection exists corresponding to strain hardening rate $\theta=d\sigma/d\varepsilon$ reaches the negative peak [27]. The true compressive stress−strain data are shown in Fig. 2, and twenty deformation conditions with distinct DRX characteristic were selected to derive the plots of θ versus σ (Fig. 3). The distinct inflections of plots in Fig. 3 indicate the onset of DRX explicitly, and the horizontal coordinate of the inflection points was considered as critical stress. In addition, the corresponding critical strains can be obtained from true stress–strain curves. The details about the solution method of critical strain ε_c and the strain for peak stress ε_p, are shown in Fig. 4. The relationships between ε_c and ε_p are summarized as Eq. (1) [28]. Equation (2) clearly shows that ε_p depends on the initial grain size d_0, deformation temperature T, strain rate $\dot{\varepsilon}$, and deformation activation energy Q_1 [28−30].

$$\varepsilon_c = a\varepsilon_p \tag{1}$$

$$\varepsilon_p = a_1 d_0^{n_1}\dot{\varepsilon}^{m_1}\exp[Q_1/(RT)] \tag{2}$$

where a is a material constant; a_1, n_1 and m_1 are material constants, which were derived from the true stress−strain data in the next section; R is the universal gas constant. Comparing with the other two dominate key factors, the influence of initial grain size on the critical strain is too feeble to be ignored in this study. Then, Eq. (2) can be simplified to

$$\varepsilon_p = a_1\dot{\varepsilon}^{m_1}\exp[Q_1/(RT)] \tag{3}$$

(1) Calculation of material constant a

From the plots of $\theta(d\sigma/d\varepsilon)$ versus σ and the true stress−strain curves, the values of ε_p and ε_c under different strain rates and temperatures are achieved, as shown in Table 1. The relationship between ε_c and ε_p is described as linear relation (Fig. 4) and the slope value of the fitted line is accepted as constant a, the concrete value is 0.35083.

(2) Calculation of material constants m_1, Q_1 and a_1

Equation (4) can be obtained by taking natural logarithms on both sides of Eq. (3):

$$\ln\varepsilon_p = \ln a_1 + m_1\ln\dot{\varepsilon} + Q_1/(RT) \tag{4}$$

According to the linear relationships of $\ln\varepsilon_p$−$\ln\dot{\varepsilon}$ (Fig. 5) at different temperatures, the material constant m_1 can be derived from the equation $m_1=\partial\ln\varepsilon_p/\partial\ln\dot{\varepsilon}$, and the concrete value is 0.101114.

According to the relationship between $\ln\varepsilon_p$ and $1/T$ (Fig. 6) under different strain rates, the material constant Q_1 can be derived from the equation $Q_1=R\partial\ln\varepsilon_p/\partial T^{-1}$, and the concrete value is 14110 J/mol. Ultimately, the constant a_1 was obtained as 0.0073 through substituting m_1 and Q_1 into Eq. (4).

Table 1 ε_p and ε_c under different temperatures and strain rates

Temperature/K	ε_p				ε_c			
	0.01 s^{-1}	0.1 s^{-1}	1 s^{-1}	10 s^{-1}	0.01 s^{-1}	0.1 s^{-1}	1 s^{-1}	10 s^{-1}
648	0.055	0.096	0.100	0.120	0.019	0.033	0.040	0.041
673	0.053	0.075	0.081	0.119	0.018	0.026	0.031	0.037
698	0.052	0.073	0.075	0.110	0.016	0.023	0.027	0.035
723	0.049	0.067	0.070	0.100	0.015	0.020	0.025	0.034
748	0.038	0.066	0.068	0.082	0.014	0.017	0.022	0.029

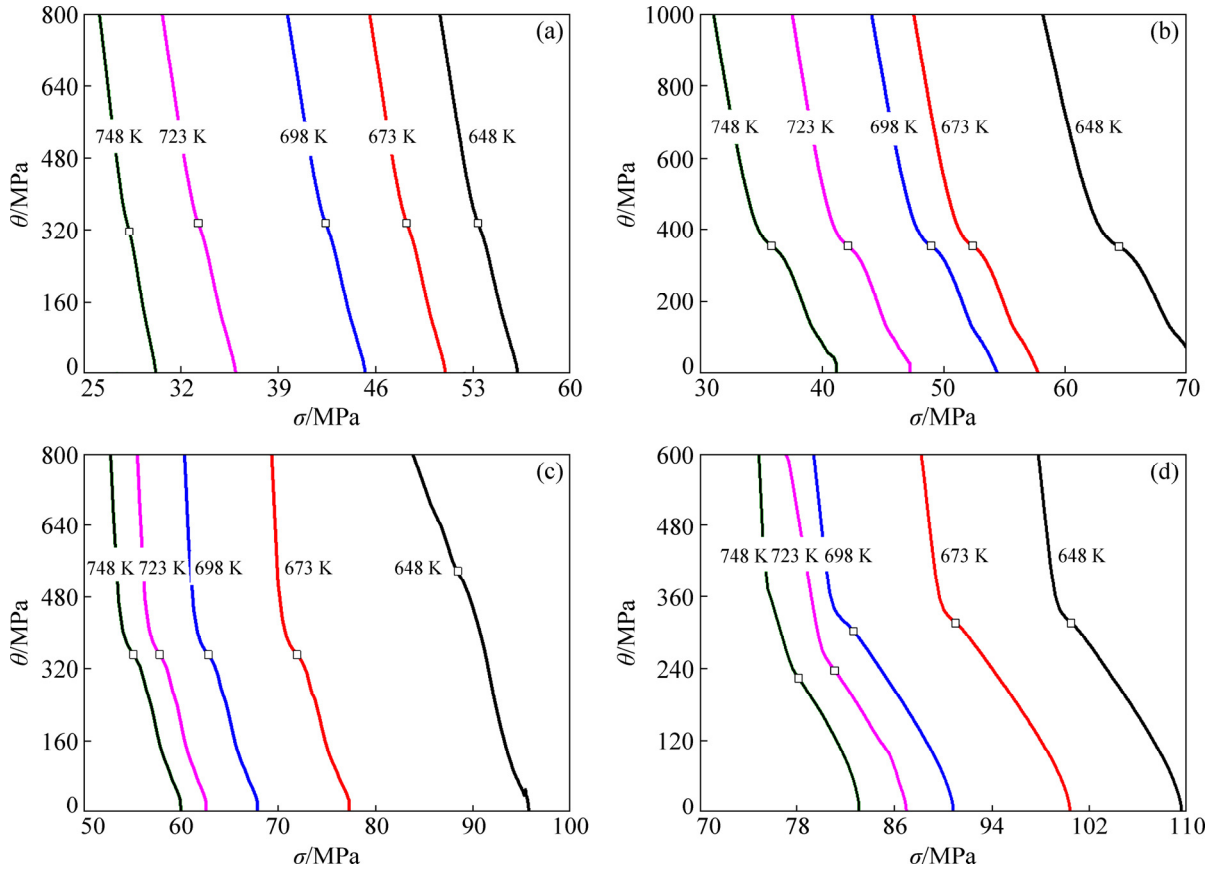

Fig. 3 θ versus σ plots under different deformation temperatures and strain rates of 0.01 s^{-1} (a), 0.1 s^{-1} (b), 1 s^{-1} (c) and 10 s^{-1} (d)

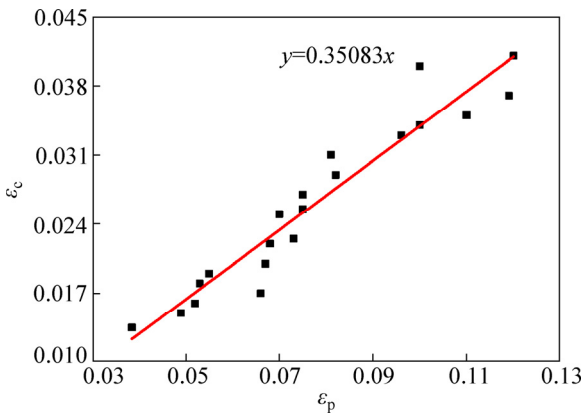

Fig. 4 Linear fitting relationship between ε_p and ε_c to obtain material constant a

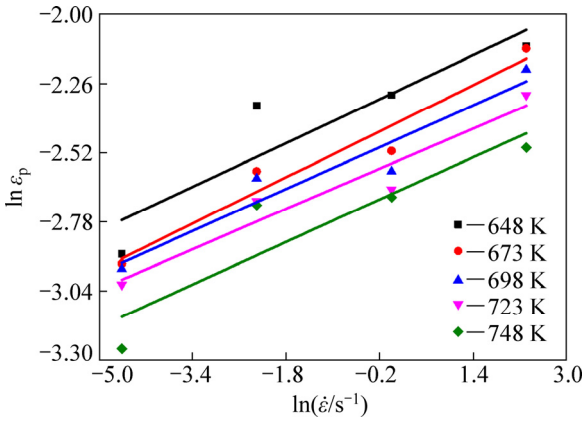

Fig. 5 Linear relationships between ln ε_p and ln $\dot{\varepsilon}$ at different temperatures

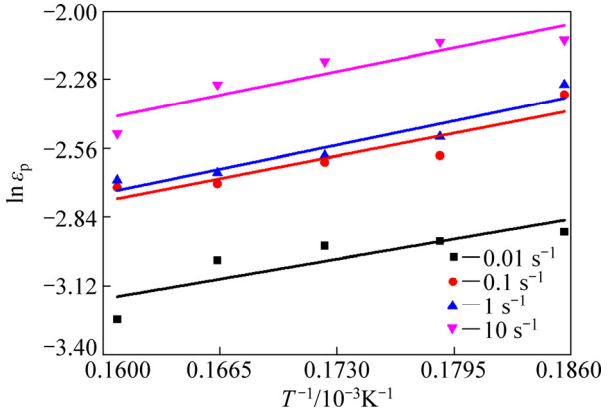

Fig. 6 Linear relationship between ln ε_p and $1/T$ under different strain rates

4.2 DRX kinetics model

During thermo-plastic deformation process, DRX nucleus form and grow up along grain boundaries, deformation bands and twin boundaries, because dislocations continually increase and pile-up. According to JMAK type equation, the evolution of the recrystallized volume fraction can be predicted by Eq. (5) [25−28], in which the true strain ε, the strain $\varepsilon_{0.5}$ and critical strain ε_c were significant parameters.

$$X_{\mathrm{DRX}}=1-\exp\left[-\beta_{\mathrm{d}}\left(\frac{\varepsilon-\varepsilon_{\mathrm{c}}}{\varepsilon_{0.5}}\right)^{k_{\mathrm{d}}}\right] \tag{5}$$

where β_d and k_d are the Avrami material constants. The strain $\varepsilon_{0.5}$ when the volume fraction of DRX reaches 50% is presented as Eq. (6) [29,30]:

$$\varepsilon_{0.5}=a_2 d_0^{n_2}\dot{\varepsilon}^{m_2}\exp[Q_2/(RT)] \tag{6}$$

where a_2, n_2 and m_2 are material constants, Q_2 is the activation energy for recrystallization, all of them can be obtained from true stress−strain curves in the next section. In this study, the true stain and strain rate were considered as the dominating parameters of the strain $\varepsilon_{0.5}$, while the initial grain size was ignored because the original average grain size of one specimen is same to others. Hence, the equation representing the strain $\varepsilon_{0.5}$ was simplified as

$$\varepsilon_{0.5}=a_2\dot{\varepsilon}^{m_2}\exp[Q_2/(RT)] \tag{7}$$

The method to determine the DRX volume fraction by microstructure is not adopted, because it needs extensive and quantitative metallography measurements under different deformation conditions. But the true stress−strain curves obtained from the isothermal compression experiment provide the valuable information about DRX. When strain ε satisfies $\varepsilon_c<\varepsilon<\varepsilon_s$ (ε_s is the steady strain when the DRX is complete), the DRX volume fraction of a material also can be calculated by [31]

$$X_{\mathrm{DRX}}=\frac{\sigma_{\mathrm{drvx}}^{\ 2}-\sigma_{\mathrm{drxx}}^{\ 2}}{\sigma_{\mathrm{drvss}}^{\ 2}-\sigma_{\mathrm{drxss}}^{\ 2}} \tag{8}$$

where σ_{drvx} and σ_{drvss} are instantaneous and steady flow stresses of the true stress−strain curve (Fig. 7) with dynamic recovery feature, σ_{drxx} and σ_{drxss} are instantaneous and steady flow stresses of the true stress−strain curve (Fig. 7) with ideal dynamic recrystallization feature.

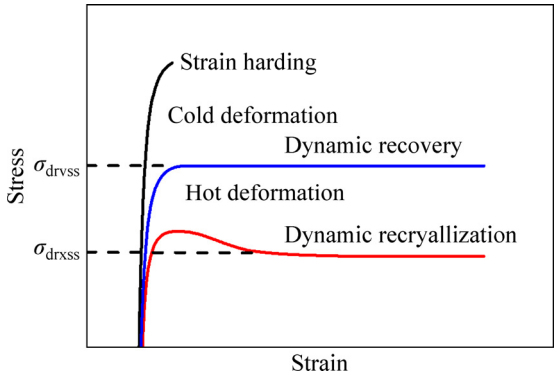

Fig. 7 Typical flow curves during cold and hot deformation

To determine X_{DRX} and $\varepsilon_{0.5}$ under different deformation conditions, the four exact parameters in Eq. (8) must be determined in advanced. As for aluminum alloys, the occurrence of DRX cannot be determined unambiguously from the shape of the flow stress curve. Therefore, the plot of θ–σ (Fig. 8) was established for defining the occurrence of DRX, from which the σ_c and σ_{drvss} were obtained [24]. Then, the σ_{drvx}, σ_{drxx} and σ_{drxss} were achieved from the stress−strain curves (Fig. 7). After a series of calculation processes, the predicted DRX volume fractions in a temperature range of 698−748 K and a strain rate range of 0.01−1 s^{-1} are shown in Fig. 9. It is noted that the DRX volume fraction nearly reaches a constant value of 1 with the increase of strain. For a fixed strain rate, the true strain

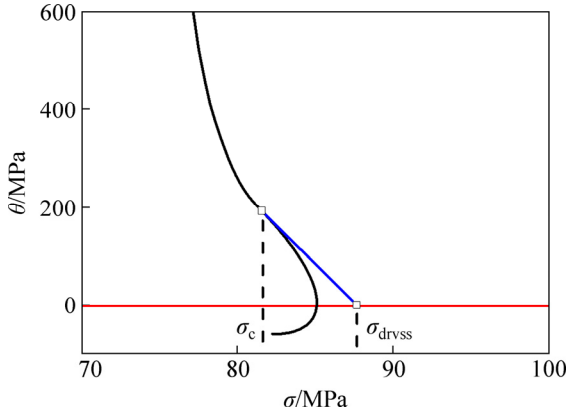

Fig. 8 Plot of θ–σ employed to determine σ_{drvss} by intercept with horizontal axis

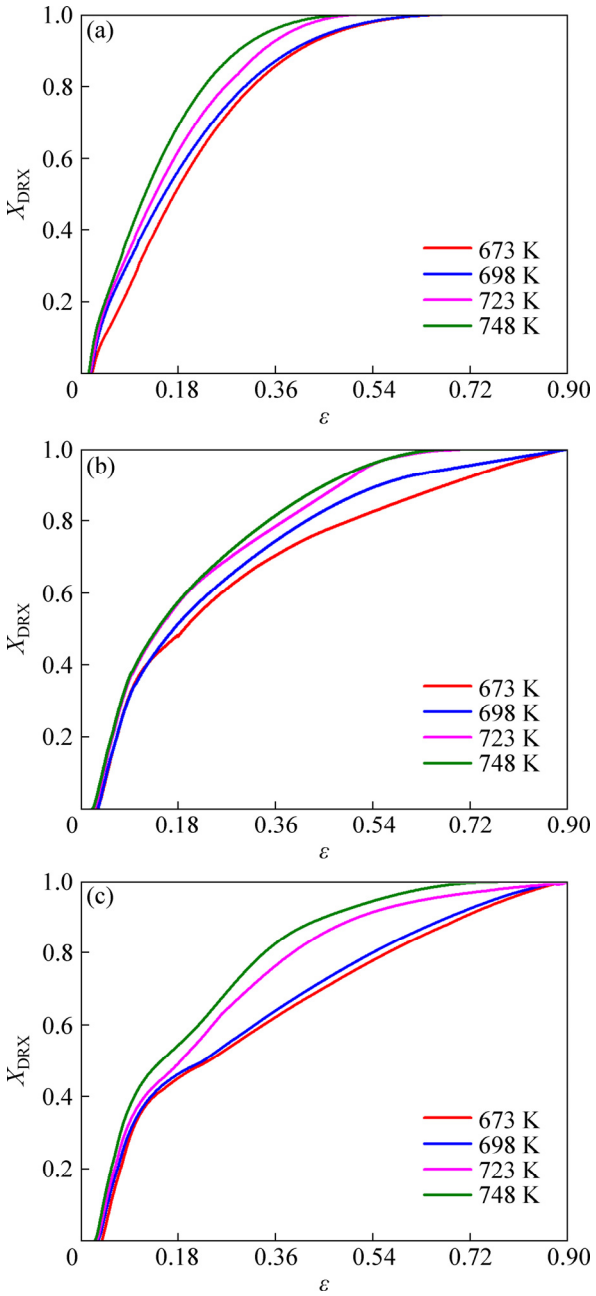

Fig. 9 Predicted DRX volume fractions in temperature range of 673−748 K at strain rates of 0.01 s^{-1} (a), 0.1 s^{-1} (b) and 1 s^{-1} (c)

required for the same amount of DRX volume fraction increases with decreasing deformation temperature, which means that DRX is delayed to a longer time. In contrast, for a fixed deformation temperature, the true strain required for the same DRX volume fraction increases with increasing strain rate. This effect can be attributed to the mobility of grain boundaries decreased with increasing strain rate and decreasing temperature. Thus, under lower strain rates and higher temperatures, the DRX volume fraction approaches to 1, which means that the deformed material tends to complete DRX.

(1) Calculation of material constants k_d and β_d

Equation (5) can be represented as Eq. (9) by taking natural logarithm on both sides of the equation:

$$\ln[-\ln(1-X_{DRX})] = \ln\beta_d + k_d \ln[(\varepsilon-\varepsilon_c)/\varepsilon_{0.5}] \quad (9)$$

Thus, the material constant k_d can be calculated by taking the partial derivative of Eq. (9). The corresponding strain $\varepsilon_{0.5}$ and critical strain ε_c have been determined on the basis of true stress−strain data. Then, the corresponding DRX volume fraction can be calculated by Eq. (8). As a series of X_{DRX}, $\varepsilon_{0.5}$, σ_c and σ have been substituted into $\ln[-\ln(1-X_{DRX})]$ and $\ln[(\varepsilon-\varepsilon_c)/\varepsilon_{0.5}]$, the relationship between them can be fitted linearly as Fig. 10. Thus, the material constants k_d and β_d were obtained as 1.51747 and 0.762889, respectively.

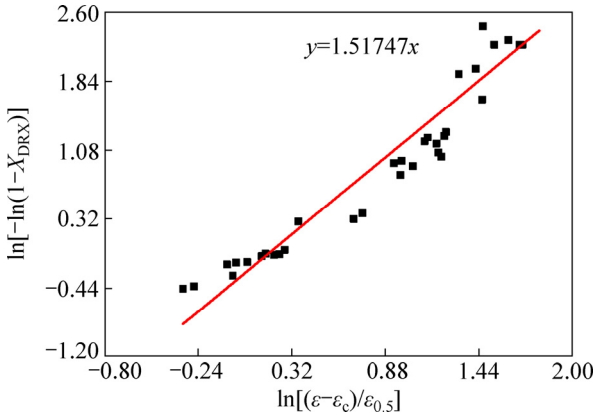

Fig. 10 Relationship between $\ln[-\ln(1-X_{DRX})]$ and $\ln[(\varepsilon-\varepsilon_c)/\varepsilon_{0.5}]$

(2) Calculation of m_2, Q_2 and a_2

Equation (10) was obtained by taking natural logarithm on both sides of Eq. (7).

$$\ln\varepsilon_{0.5} = \ln a_2 + m_2 \ln\dot{\varepsilon} + Q_2/(RT) \quad (10)$$

From Eq. (10), it can be derived that $m_2 = \partial\ln\varepsilon_{0.5}/\partial\ln\dot{\varepsilon}$, $Q_2 = R\partial\ln\varepsilon_{0.5}/\partial T^{-1}$. The stress $\sigma_{0.5}$ when 50% DRX occurred can be calculated by Eq. (8), then the corresponding strain $\varepsilon_{0.5}$ can be found in the true stress−strain data. According to the values of $\varepsilon_{0.5}$ under various deformation conditions, the plots of $\ln\varepsilon_{0.5} - \ln\dot{\varepsilon}$ and $\ln\varepsilon_{0.5} - 1/T$ are shown in Figs. 11 and 12, respectively. After linear regression fitting and averaging, the material constants are calculated as: m_2=0.074815, Q_2=26920.7 J/mol. Substituting m_2 and Q_2 into Eq. (10) can obtain different twelve values of material constant a_2, under four strain rates and three temperatures, and the mean value is considered as the material constant a_2, the concrete value is 0.00854489.

5 Analysis of DRX fraction by finite element method

The true stress−strain data achieved from isothermal tests and the developed DRX kinetic equation were

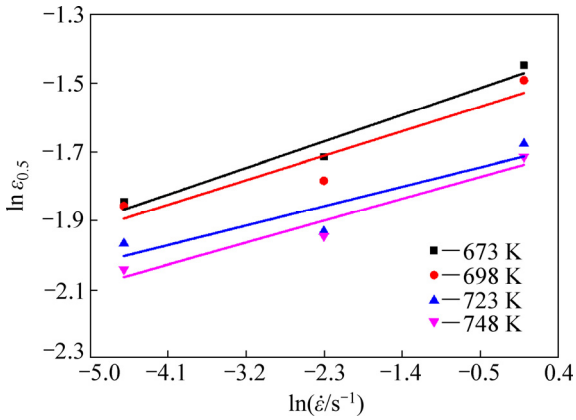

Fig. 11 Linear fitting relationship between $\ln \varepsilon_{0.5}$ and $\ln \dot{\varepsilon}$ to obtain material constant m_2

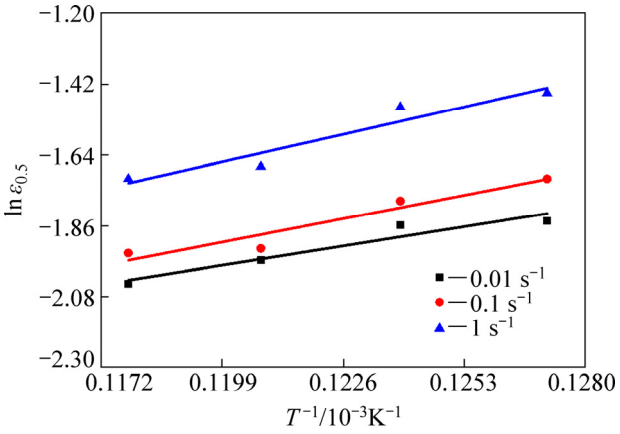

Fig. 12 Linear fitting relationship between $\ln \varepsilon_{0.5}$ and $1/T$ to obtain deformation active energy

programed into finite element codes on DEFORM-3D platform. And then, an FE simulation model, displayed the forming process of a preformed blank dynamically, was established. During a large plastic deformation of workpiece at a high temperature, the elastic deformation is usually negligible. Thus, in the FE simulation, the workpiece was set as rigid−plastic body, and the tools were set as rigid body. In addition, a half of the symmetry specimen is given as a deformation model based on the consideration of reducing the time of finite element simulate. It should be noticed that the friction at the contact interfaces between workpiece and tools was set as shear type, and the value was selected as 0.3. As a series of compressions in agreement with experimental conditions had been simulated, the DRX volume fraction distribution in deformed materials was revealed.

The DRX volume fraction of deformation specimen under the temperature of 723 K and the strain rate of 0.1 s^{-1} were taken as the example to discuss the influence of true strain. With the increase of true strain, the average DRX volume fractions in relevant deformation degree gradually increase, as shown in Fig. 13. Moreover, the DRX appears in the center region of cylindrical billet primarily, and then increases and extends along the symmetric line.

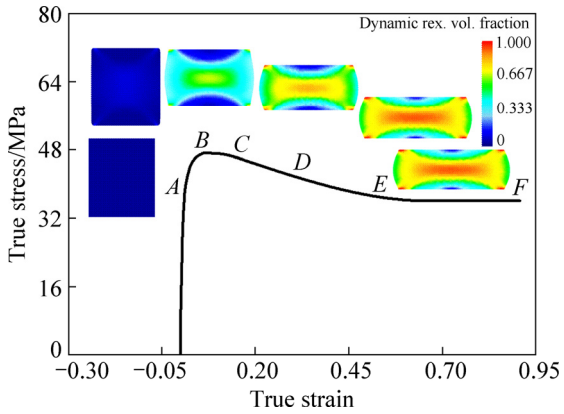

Fig. 13 Evolution of DRX volume fraction with increasing true strain

From the DRX kinetics model, the DRX volume fraction was considered as a function of the deformation conditions. The results of the present finite simulation data (Fig. 14) clearly show the relationship between the DRX volume fraction distribution and temperature under deformation strain rate of 1 s^{-1} and deformation degree of 60% (reduction in height). For this specific strain rate, the average DRX volume fraction rises from 0.45 to 0.683 with the increase of temperature. Figure 15 shows the relationship between the DRX volume fraction distributions and strain rates under deformation temperature of 723 K. It is noted that the average DRX volume fraction decreases from 0.766 to 0.532 with the increase of strain rate. Because the nonlinearly interactions of strain field, strain rate field and temperature field are inhomogeneous, the distribution of DRX volume fraction is inhomogeneous in the deformed material, as clearly shown in Figs. 14 and 15. The maximum DRX volume fraction usually locates at the central region of the billet, while the minimum DRX volume fraction locates at the central region on the two end surfaces with a downward trend.

The histories of microstructural evolution during the whole hot forming processes for AlCu4SiMg alloy can be uncovered and described numerically through the FE simulation. Meanwhile, the results of FE simulation confirm that the theoretical DRX kinetics model can be successfully incorporated into the FE model to predict and observe the microstructural evolution of hot upsetting process. Hence, the FE simulation with DRX kinetics model can be utilized to guide actual process, which will gradually replace the traditional time-consuming trial-and-error approach.

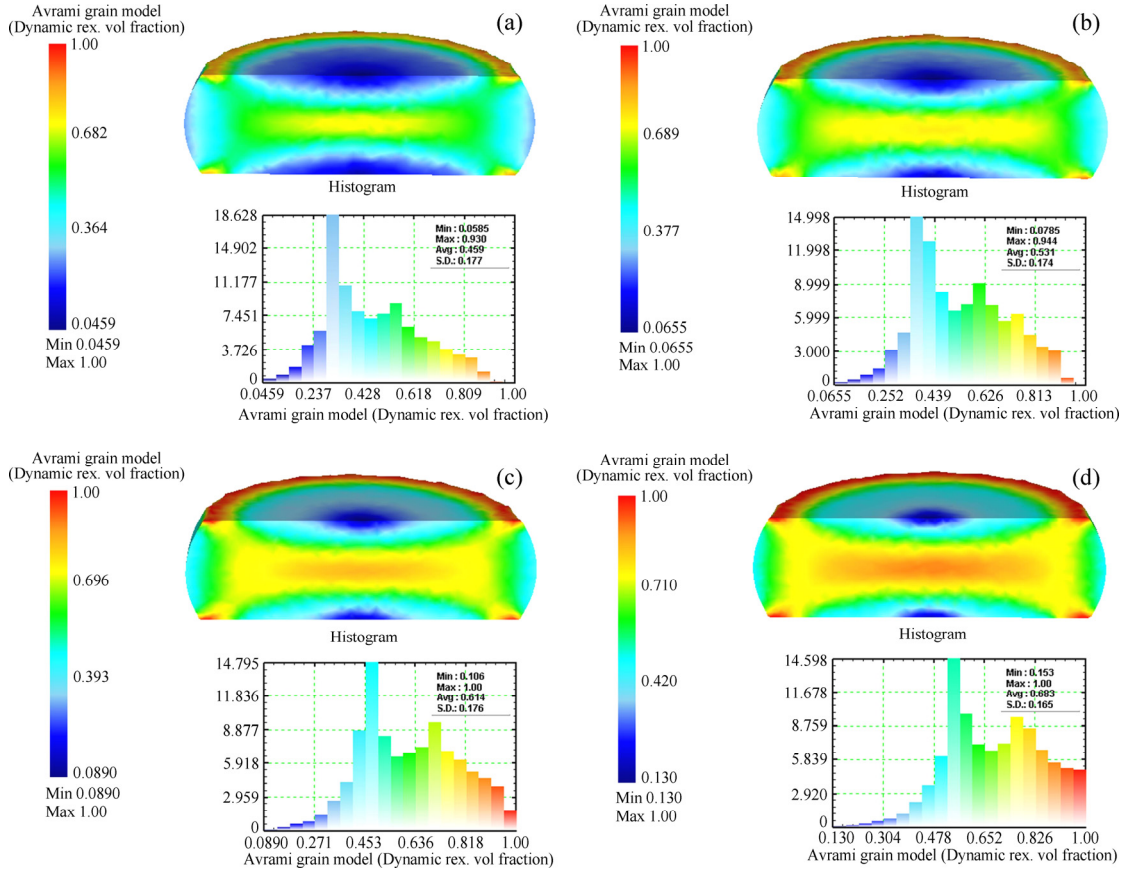

Fig. 14 DRX volume fractions under strain rate of 1 s^{-1} at temperatures of 673 K (a), 698 K (b), 723 K (c) and 748 K (d)

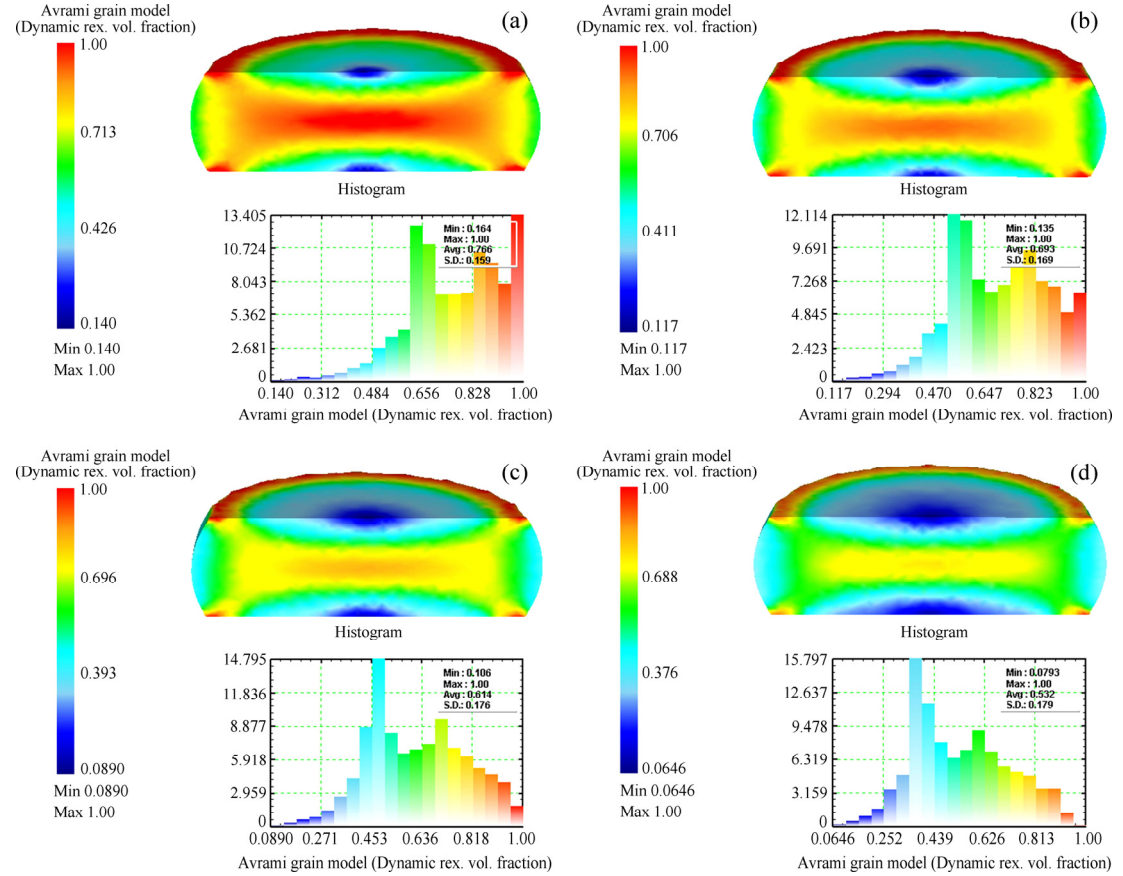

Fig. 15 DRX volume fractions at temperature of 723 K under strain rates of 0.01 s^{-1} (a), 0.1 s^{-1} (b), 1 s^{-1} (c) and 10 s^{-1} (d)

6 Microstructure

Observing the microstructures of deformed specimens (Fig. 16) is a universal method to quantify the results of microstructural evolution. To observe the microstructure of deformed specimen across-the-board under a fixed strain rate of 1 s^{-1} at 723 K, the microstructures of different three regions P1−P3 (Fig. 17) on the section plane of the deformed specimen are shown in Figs. 18(b−d). The microstructure of end surface (P1) is thick dendrite with diminutive deformation, which is more similar to original as-cast texture shown in Fig. 18(a). As compared with the end surface (P1), the microstructure of central region (P3) illustrates that the deformation extent is significantly enhanced. The orientation of deformation crystal has a trend to along the radial direction of specimen as the deformation proceeds. The flow localization disappears and the uniform elongated grains appear in the microstructures, which show the typical features of dynamic recovery. As can be seen from Figs. 18(b) and (c), the extent of dynamic recrystallization at the end region is weaker than that at the central region, which brings about the inhomogeneity of the microstructure. The cause lies in the fact that the deform degree of the material is inhomogeneous, which directly affects the DRX volume fraction distribution of deformation material.

It is most widely accepted that the usual deformation mechanisms of AlCu4SiMg are DRV, DRX and super-plasticity, which are impacted by the deformation parameters such as strain rate and temperature. In Fig. 19, the microstructures of the central region with DRX grains on the section plane at strain

Fig. 16 Contrast structure pictures of specimens before and after experiments

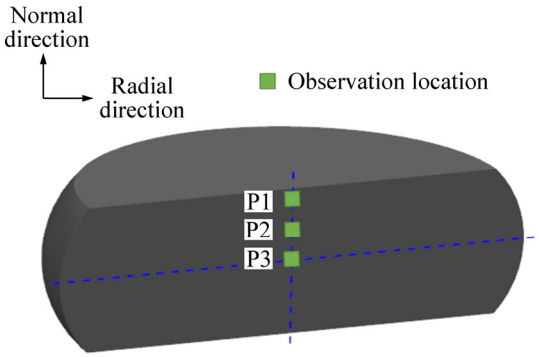

Fig. 17 Three regions (P1−P3) selected for microstructure observation

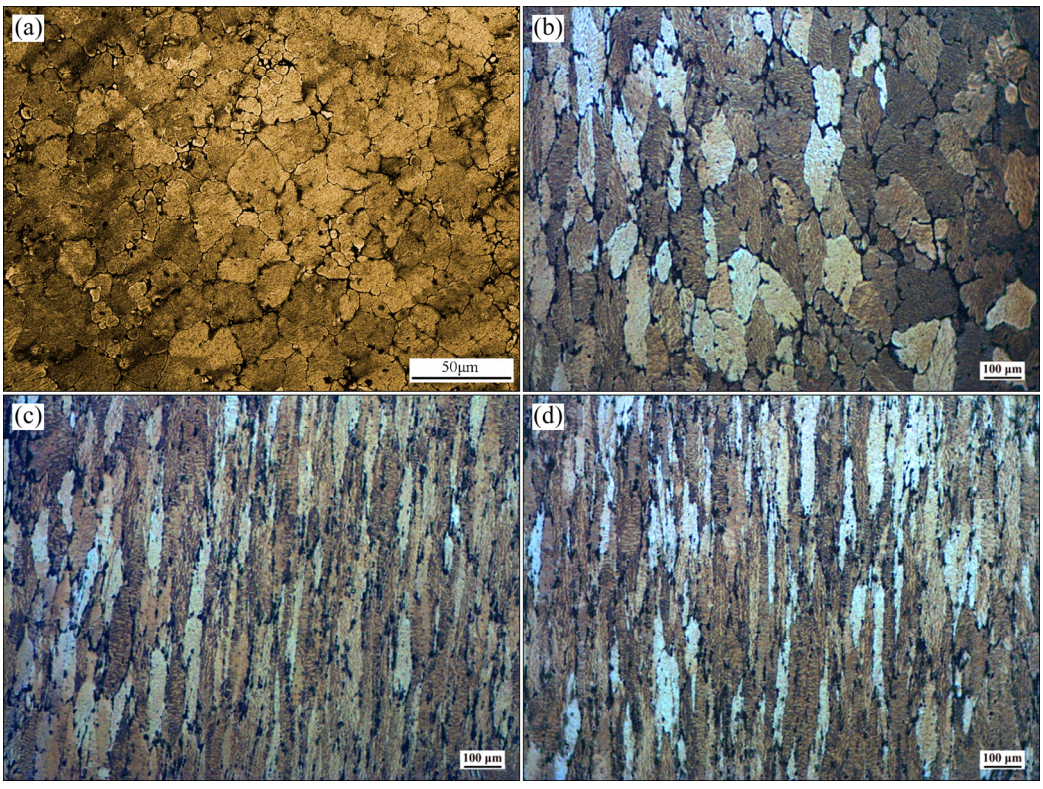

Fig. 18 Microstructures of original cast texture (a), and regions P1 (b), P2 (c), P3 (d) on section plane of deformed specimen

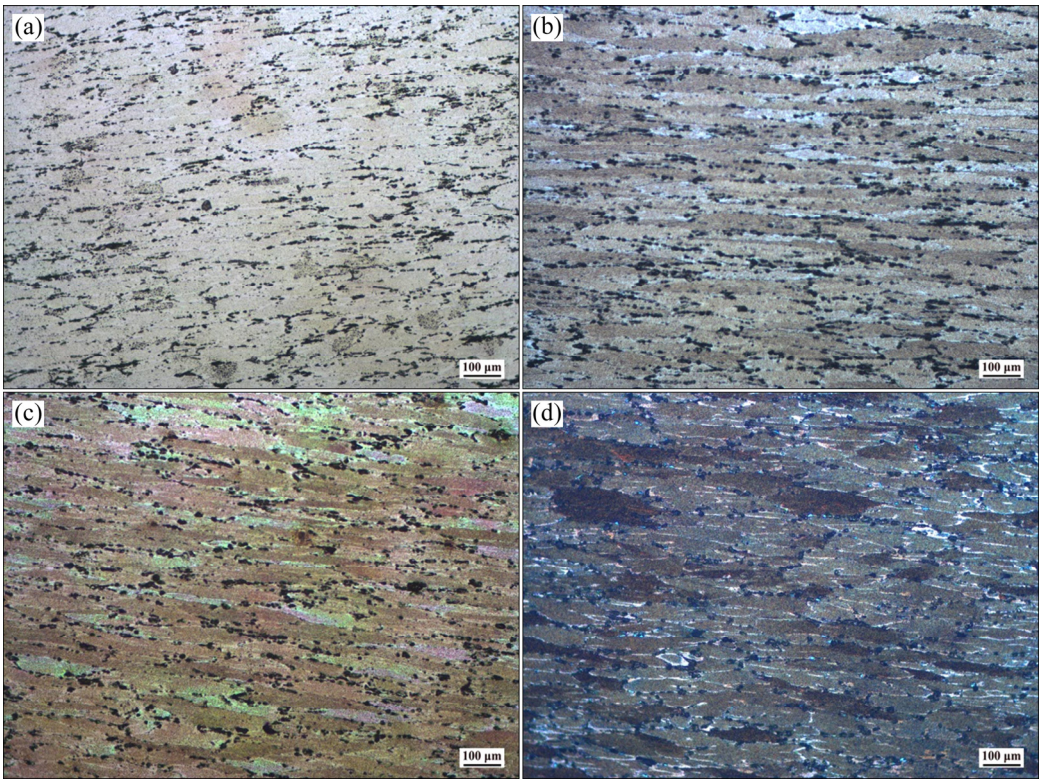

Fig. 19 Microstructures at temperature of 723 K and strain rates of 0.01 s^{-1} (a), 0.1 s^{-1} (b), 1 s^{-1} (c) and 10 s^{-1} (d)

rates of 0.01−10 s^{-1} and temperature of 723 K are shown distinctly. During hot forming, the precipitated second phases such as Al_3Zr and $Al_{20}Cu_2Mn_3$ contribute to pin the dislocations effectively. At higher strain rates, it can be noted that the fine recrystallized grains can be found along with the banded grain boundaries. With the decrease of strain rate, the number of the recrystallized grains with wavy or corrugated grain boundaries increase and the size of grains becomes uniform. This is due to the fact that lower strain rate provides longer time for the diffusion of atoms, slip of dislocation and migration of grain boundaries.

As for 1 s^{-1}, the microstructures of the central region which disclose the influence of the deformation temperature on deformation material are shown in Fig. 20. At lower temperatures, recrystallization microstructure transformed from the original grains is nearly inexistent. With the increase of the deformation temperature, the number of deformation band in deformed material increases and the slip of dislocation is reinforced, which result in greater deformation of grains and stronger DRV. When the temperature reaches 698 K, the fine recrystallized grains occur in the interior of deformed material. With increasing temperature, the number of the fine recrystallized grains rises, and the grain size becomes more and more homogeneous. The degree of dynamic recrystallization presents an escalating trend due to higher mobility of grain boundaries (growth kinetics). When the deformation temperature reaches 748 K, the dynamic recrystallization was completed at incipient compression stage, and then the new grains have been compressed to banded structure. It is worth emphasizing that the recrystallized grain size has increased gradually with increasing temperature, and all the grains tend to be more and more homogeneity because of stronger adaptivity for grain boundary migration.

7 Conclusions

(1) During isothermal deformation, the stress−strain curves of AlCu4SiMg alloy indicate three distinct stages. With deformation temperature increasing, the critical stress decreases under a constant strain rate. Inversely, it increases while increasing strain rate at a fixed temperature.

(2) The kinetic model of DRX including the deformation parameters' effects was established. And the evolution model of DRX volume fraction can be concluded as follows: the strain required for the same DRX volume fraction increases with decreasing the deformation temperature under a fixed strain rate, on the contrary, it increases with increasing strain rate at a fixed temperature.

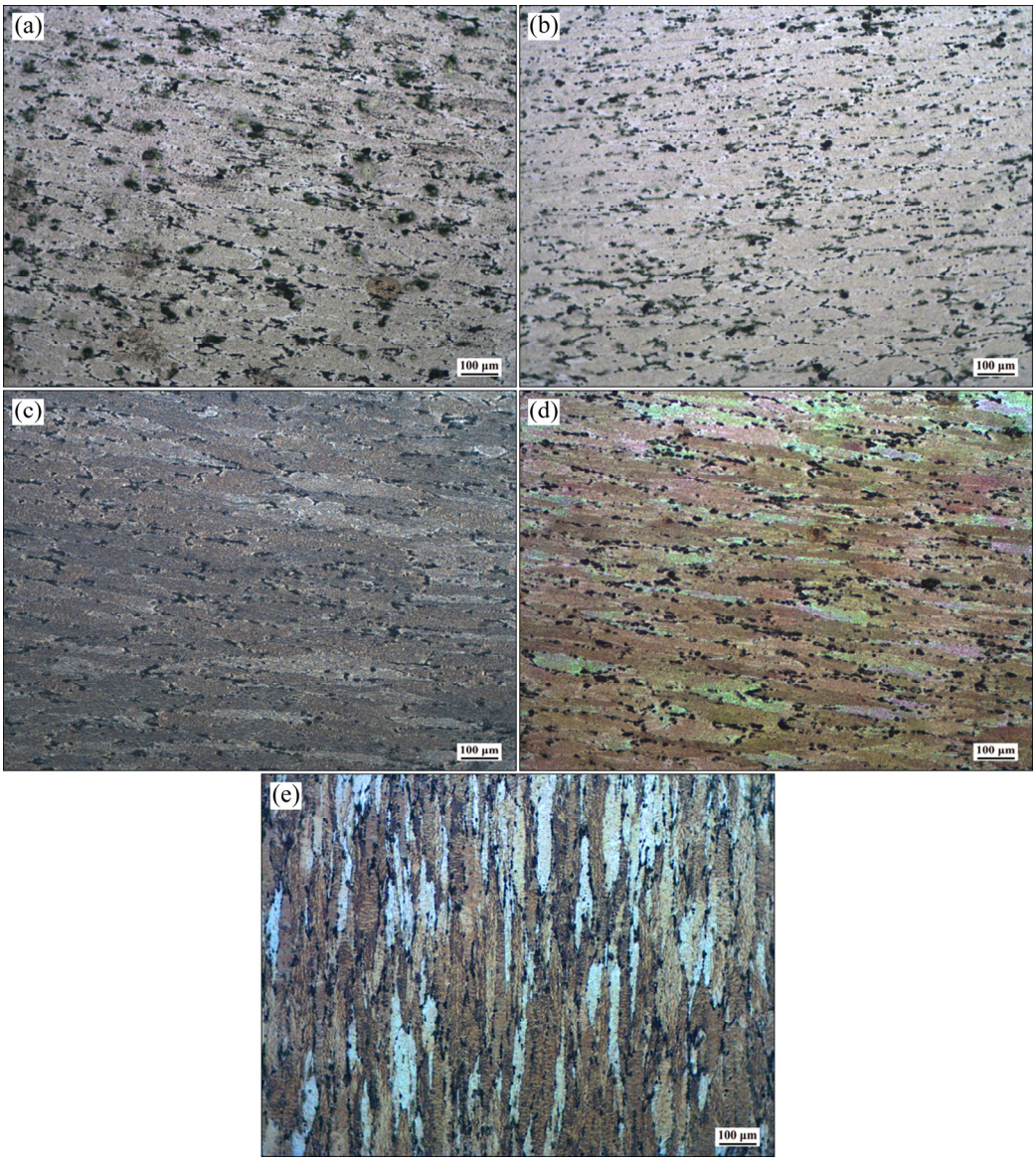

Fig. 20 Microstructures at strain rate of 1 s^{-1} and different temperatures of 648 K (a), 673 K (b), 698 K (c), 723 K (d) and 748 K (e)

(3) From the FE simulation results, the DRX volume fraction distributions were various under different deformation conditions. It increases with decreasing the strain rate and increasing the deformation temperature, which is completely in conformity with the evolution law of DRX volume fraction.

(4) According to the microstructural observations of deformed specimens, the theoretical predictions and numerical results of DRX volume fraction were verified.

References

[1] OKAYASU M, SATO K, MIZUNO M. A new etching technique for revealing the plastic deformation zone in an Al−Cu−Mg alloy [J]. Journal of Materials Science, 2008, 43(8): 2792−2798.

[2] PAREL T S, WANG S C, STARINK M J. Hardening of an Al–Cu–Mg alloy containing Types I and II S phase precipitates [J]. Materials & Design, 2010, 31(Suppl 1): S2−S5.

[3] HUANG K, LOG R E. A review of dynamic recrystallization phenomena in metallic materials [J]. Materials & Design, 2016, 111: 548−574.

[4] DOHERTY R D, HUGHES D A, HUMPHREYS F J, JONAS J J, JENSEN D J, KASSNER M E, KING W E, MCNELLEY T R, MCQUEEN H J, ROLLETT A D. Current issues in recrystallization: A review [J]. Materials Science & Engineering A, 1997, 238(2): 219-274.

[5] SAKAI T, BELYAKOV A, KAIBYSHEV R, MIURA H, JONAS J J. Dynamic and post-dynamic recrystallization under hot, cold and severe plastic deformation conditions [J]. Progress in Materials Science, 2014, 60(1): 130−207.

[6] WOO W, CHOO H, PRIME M B, FENG Z, CLAUSEN B. Microstructure, texture and residual stress in a friction-stir-processed AZ31B magnesium alloy [J]. Acta Materialia, 2008, 56(8): 1701−1711.

[7] KAIBYSHEV R, MALOPHEYEV S. Mechanisms of dynamic

recrystallization in aluminum alloys [J]. Materials Science Forum, 2014, 794−796: 784−789.

[8] QUAN Guo-zheng, MAO An, LUO Gui-chang, LIANG Jian-ting, WU Dong-sen, ZHOU Jie. Constitutive modeling for the dynamic recrystallization kinetics of as-extruded 3Cr20Ni10W2 heat-resistant alloy based on stress−strain data [J]. Materials & Design, 2013, 52(24): 98−107.

[9] QUAN Guo-zheng, LUO Gui-chang, LIANG Jian-ting, WU Dong-sen, MAO An, LIU Qing. Modelling for the dynamic recrystallization evolution of Ti−6Al−4V alloy in two-phase temperature range and a wide strain rate range [J]. Computational Materials Science, 2015, 97: 136−147.

[10] LI Yu-fei, WANG Zhen-hong, ZHANG Lin-ying, LUO Chao, LAI Xin-chun. Arrhenius-type constitutive model and dynamic recrystallization behavior of V−5Cr−5Ti alloy during hot compression [J]. Transactions of Nonferrous Metals Society of China, 2015, 25(6): 1889−1900.

[11] ZHOU Mi, LIN Yong-cheng, DENG Jiao, JIANG Yu-qiang. Hot tensile deformation behaviors and constitutive model of an Al−Zn−Mg−Cu alloy [J]. Materials & Design, 2014, 59(6): 141−150.

[12] CAI Zhi-wei, CHEN Fu-xiao, MA Feng-jie, GUO Jun-qing. Dynamic recrystallization behavior and hot workability of AZ41M magnesium alloy during hot deformation [J]. Journal of Alloys & Compounds, 2016, 670(3): 55−63.

[13] WEN Dong-xu, LIN Yong-cheng, ZHOU Ying. A new dynamic recrystallization kinetics model for a Nb containing Ni−Fe−Cr-base superalloy considering influences of initial δ phase [J]. Vacuum, 2017, 14: 316−327.

[14] CHEN Ming-song, LIN Yong-cheng, LI Kuo-kuo, ZHOU Ying. A new method to establish dynamic recrystallization kinetics model of a typical solution-treated Ni-based superalloy [J]. Computational Materials Science, 2016, 122: 150−158.

[15] LI Peng-wei, LI Hui-zhong, HUANG Lan, LIANG Xiao-peng, ZHU Ze-xiao. Characterization of hot deformation behavior of AA2014 forging aluminum alloy using processing map [J]. Transactions of Nonferrous Metals Society of China, 2017, 27(8): 1677−1688.

[16] LI Dong-feng, ZHANG Duan-zheng, LIU Sheng-dan, SHAN Zhao-jun, ZHANG Xin-ming, WANG Qin, HAN Su-qi. Dynamic recrystallization behavior of 7085 aluminum alloy during hot deformation [J]. Transactions of Nonferrous Metals Society of China, 2016, 26(6): 1491−1497.

[17] LI Hui-zhong, LIU Ruo-mei, LIANG Xiao-peng, DENG Min, LIAO Hui-juan, HUANG Lan. Effect of pre-deformation on microstructures and mechanical properties of high purity Al-Cu-Mg alloy [J]. Transactions of Nonferrous Metals Society of China, 2016, 26(6): 1482−1490.

[18] DHAL A, PANIGRAHI S K, SHUNMUGAM M S. Insight into the microstructural evolution during cryo-severe plastic deformation and post-deformation annealing of aluminum and its alloys [J]. 2017, 726: 1205−1219.

[19] LI Bo, PAN Qing-lin, YIN Zhi-min. Characterization of hot deformation behavior of as-homogenized Al–Cu–Li–Sc–Zr alloy using processing maps [J]. Materials Science & Engineering A, 2014, 614(4): 199−206.

[20] TAJALLY M, HUDA Z. Recrystallization kinetics for aluminum alloy 7075 [J]. Metal Science & Heat Treatment, 2011, 53(5−6): 213−217.

[21] CHENG Yong-qi, ZHANG Hui, CHEN Zhen-hua, XIAN Kui-feng. Flow stress equation of AZ31 magnesium alloy sheet during warm tensile deformation [J]. Journal of Materials Processing Technology, 2008, 208(1): 29−34.

[22] QUAN Guo-zheng, SHI Yu, WANG Yi-xin, KANG B S, KU T W, SONG W J. Constitutive modeling for the dynamic recrystallization evolution of AZ80 magnesium alloy based on stress–strain data [J]. Materials Science & Engineering A, 2011, 528(28): 8051−8059.

[23] LIN Yong-Cheng, DENG Jiao, JIANG Yu-Qiang, WEN Dong-Xu, LIU Guan. Hot tensile deformation behaviors and fracture characteristics of a typical Ni-based superalloy [J]. Materials & Design, 2014, 55(6): 949−957.

[24] HSIAO I C, HUANG J C. Deformation mechanisms during low-and high-temperature superplasticity in 5083 Al-Mg alloy [J]. Metallurgical & Materials Transactions A, 2002, 33(5): 1373−1384.

[25] LIAO X Z, HUANG J Y, ZHU Y T, ZHOU F, LAVERNIA E J. Nanostructures and deformation mechanisms in a cryogenically ball-milled Al−Mg alloy [J]. Philosophical Magazine, 2003, 83(26): 3065−3075.

[26] YAO Li, LIU Zhi-yi, LIN Liang-hua, PENG Jiang-tao, NING Ai-lin. Deformation behavior of an Al−Cu−Mg−Mn−Zr alloy during hot compression [J]. Journal of Materials Science, 2011, 46(11): 3708−3715.

[27] YANG Z, GUO Y C, LI J P, HE F, XIA F, LIANG M X. Plastic deformation and dynamic recrystallization behaviors of Mg−5Gd−4Y−0.5Zn−0.5Zr alloy [J]. Materials Science & Engineering A, 2008, 485(1−2): 487−491.

[28] WANG K L, FU M W, LU S Q, LI X. Study of the dynamic recrystallization of Ti−6.5Al−3.5Mo−1.5Zr−0.3Si alloy in β-forging process via Finite Element Method modeling and microstructure characterization [J]. Materials & Design, 2011, 32(3): 1283−1291.

[29] JI Guo-liang, LI Fu-guo, LI Qing-hua, LI Hui-qu, LI Zhi. Research on the dynamic recrystallization kinetics of Aermet100 steel [J]. Materials Science & Engineering A, 2010, 527(9): 2350−2355.

[30] LIN Yong-cheng, CHEN Ming-Song, ZHONG Jue. Effects of deformation temperatures on stress/strain distribution and microstructural evolution of deformed 42CrMo steel [J]. Materials & Design, 2009, 30(3): 908−913.

[31] ZAHIRI S H, DAVIES C H J, HODGSON P D. A mechanical approach to quantify dynamic recrystallization in polycrystalline metals [J]. Scripta Materialia, 2005, 52(4): 299−304.

AlCu4SiMg 合金的动态再结晶体积分数模型构建及其在有限元模型中的应用

权国政[1]，施瑞菊[1]，赵 江[1]，刘 乔[1]，熊 威[2]，邱慧敏[1]

1. 重庆大学 材料科学与工程学院 机械传动国家重点实验室，重庆 400044；
2. 清华大学 核能与新能源技术研究院 先进核能技术协同创新中心
先进反应堆工程与安全教育部重点实验室，北京 100084

摘 要：为了更好地剖析 AlCu4SiMg 合金的动态再结晶（DRX）行为和流变行为的耦合效应，实施了具有 DRX 演变模型的有限元模拟。利用 Gleeble−3500 热模拟试验机，在温度为 648~748 K，应变速率为 0.01~10 s^{-1} 的变形条件下对该合金进行等温压缩实验。依据实验所得的真实应力−应变数据，拟合应变硬化率曲线(表征 $d\sigma/d\varepsilon$ 与 σ 之间的关系)，并识别产生动态再结晶时的临界应变值(ε_c)。通过对材料参数的求解，确定 DRX 的体积分数方程和 DRX 达到 50%时的应变方程。构建 DRX 体积分数演变的有限元(FE)模型，对一系列等温压缩实验进行模拟仿真。DRX 体积分数演变可视化结果显示：在同一应变速率条件下，达到相同 DRX 体积分数的应变量随温度的降低而增加；在同一温度条件下，该应变量随应变速率的增加而增加。最后，通过金相分析验证 AlCu4SiMg 合金的 DRX 动力学模型及有限元模拟结果的可靠性。

关键词：AlCu4SiMg 合金； DRX 动力学模型；DRX 体积分数；流变行为

(Edited by Xiang-qun LI)